



Orbital and millennial northern mid-latitude westerlies over the last glacial period

Yun Li^{1,2,3,4} · Yougui Song³ · Qiuzhen Yin⁴ · Li Han^{1,2} · Yixuan Wang^{1,2}

Received: 4 December 2018 / Accepted: 26 February 2019 / Published online: 19 March 2019
© Springer-Verlag GmbH Germany, part of Springer Nature 2019

Abstract

The northern mid-latitude westerlies play an important role in the climate interactions between the low and high latitudes. Our understanding of the factors that control the latitudinal displacement of the westerlies remains incomplete due to insufficient climatic proxy. Here we present a latitudinal-shift record of the westerlies in the eastern Central Asia over the past 70,000 years, on the basis of the grain size of the loess sequence from the Tacheng basin. On millennial timescale, the variation of the reconstructed westerlies resembles that of the Greenland temperature and the Atlantic meridional overturning circulation (AMOC), indicating the role of the AMOC on the westerlies. On orbital time scale, their variation is controlled by precession and insolation. Our analyses of the LOVECLIM and CCSM3 models' results show that the impact of insolation and AMOC on the latitudinal shift of the westerlies is through changing the latitudinal temperature and pressure gradients.

Keywords Orbital · Millennial · Northern westerlies · AMOC · Precession

1 Introduction

The mid-latitude westerlies are the prevailing eastward winds extending from the earth's surface up to the stratosphere in both hemispheres. As one of the major components of the large-scale atmospheric circulations, westerlies exert a considerable influence on the global climate by modulating

the transport and distribution of momentum, heat, and moisture. They are products of baroclinic instability that develop particularly intensely in winter due to the strong pole-to-equator temperature gradient (Son and Lee 2005). Changes in the position and intensity of the westerly jets associated with storm tracks play a key role in reshaping precipitation patterns in middle latitudes (Yin 2005).

The last glacial period was characterized by a series of rapid millennial-scale climatic oscillations referred as the Dansgaard–Oeschger abrupt events which are best defined in the Greenland ice core records (Dansgaard et al. 1993). These events can be linked to the Atlantic meridional overturning circulation (AMOC) at diverse regions on millennial timescale (Clement and Peterson 2008; Sun et al. 2012). In addition, the westerlies also transmits the high-latitude North Atlantic signals to mid-latitude regions (Li et al. 2016b). They encompass a large meridional domain controlling climatic changes in Europe (Brauer et al. 2008) and Central Asia (Li et al. 2016b) (Fig. 1). Many modelling and proxy studies have contributed to the understanding of the AMOC, but few on the mid-latitude westerlies. Especially, the evolution history of the westerlies is less well understood due to insufficient paleoclimate records. To better know the variations of the mid-latitude westerlies on millennial and orbital timescales and their forcing mechanisms, we reconstructed the latitudinal-shift variations of

✉ Yun Li
liyun@isl.ac.cn

✉ Yougui Song
syg@ieccas.cn

✉ Qiuzhen Yin
qiuzhen.yin@uclouvain.be

¹ Key Laboratory of Comprehensive and Highly Efficient Utilization of Salt Lake Resources, Qinghai Institute of Salt Lakes, Chinese Academy of Sciences, 18 Xining Road, Xining 810008, China

² Qinghai Provincial Key Laboratory of Geology and Environment of Salt Lake, Qinghai Institute of Salt Lakes, Chinese Academy of Sciences, Xining 810008, China

³ State Key Laboratory of Loess and Quaternary Geology, Institute of Earth Environment, Chinese Academy of Sciences, Xi'an 710061, China

⁴ Georges Lemaître Centre for Earth and Climate Research, Earth and Life Institute, Université Catholique de Louvain, 1348 Louvain-La-Neuve, Belgium

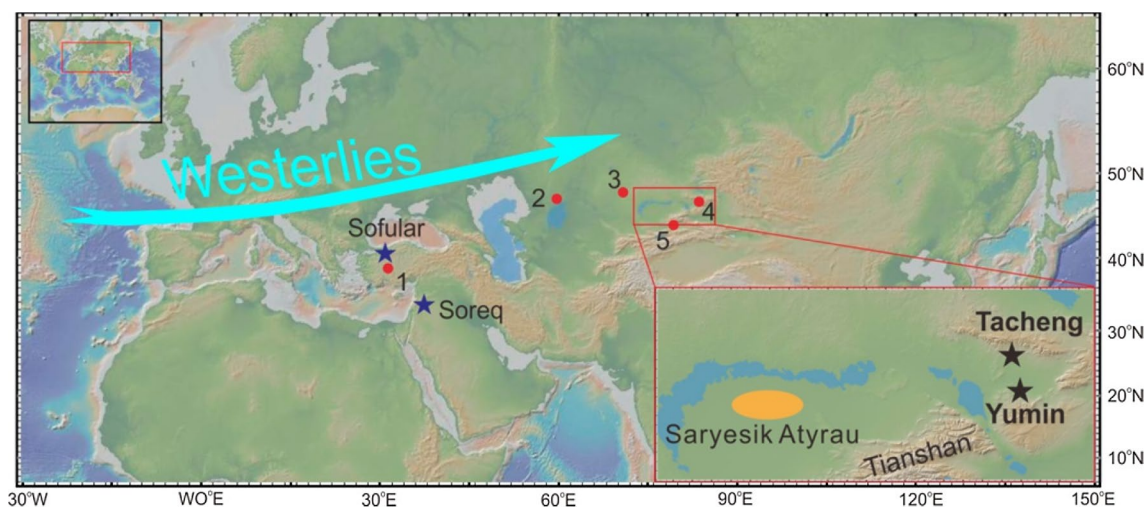


Fig. 1 Loess sections, meteorological station and cave locations (the insert shows the map position in the world). Black star is for Tacheng loess, blue stars for Sofular and Soreq Caves, red dots for meteorological stations from National Climatic Data Center (<http://www.climate.gov/data/maps-and-data#>) and China meteorological data net-

work (<http://data.cma.cn/>): 1—Ankara; 2—Aral Sea; 3—Kzyl-Zar; 4—Tacheng; 5—Yining; light orange ellipse indicates the Saryesik Atyrau desert (S). Light blue arrow depicts wind directions of the westerlies

the northern westerlies during the last 70,000 years based on two high-resolution loess records in eastern Central Asia. The optically stimulated luminescence (OSL) analyses were performed to provide an independent chronology to assess the latitudinal shifts of rapid westerlies. Furthermore, we combine loess, speleothem and sea ice records with model simulations to investigate the physical mechanisms of millennial- and orbital-scale variations of the westerlies.

2 Geographical settings and loess sequences

The Tacheng basin, situated at the eastern Central Asia, is a suitable place for reconstructing the past variability of the mid-latitude westerlies because the precipitation and dust transportation in this basin are almost entirely controlled by the westerlies (Figs. 1, 2). Figure 2 shows that similar to other westerlies-dominating regions, the dominant precipitation seasons at Tacheng are spring and winter. The moisture there is mainly transported from the Atlantic Ocean, Mediterranean Sea, Black Sea and Caspian Sea by the westerlies (Aizen et al. 1996). Moreover, dust storms prevail in the Tacheng region from April to October, mainly during the dry summer season. To explain the relationship between the dust storms in the Tacheng and atmospheric circulation, we made the correlation between dust storm day anomalies, the sea ice index and the previous winter/summer North Atlantic Oscillation (NAO) index (Fig. 3), which are a major source of interannual climate change in the Northern Hemisphere (Hurrell and Van Loon 1997). The high positive correlation

between the winter NAO index and the dust storm day in the Tacheng during 1966–1989 showed the winter NAO index is a main factor for dust storm outbreaks over the Tacheng by the transmit of the westerlies, while the lower correlation during 1990–2005 maybe be attributed to a pronounced decrease of sea ice (Zhang et al. 2006). Our two-loess section Tacheng (TC) (N46°53', E82°58') and Yumin (YM) (N46°12', E82°54') are about 300 km away from the modern Saryesik Atyrau Desert margin and are situated in the depocenter of the modern dust storms (Fig. 1). At present, the Saryesik Atyrau Desert is the main source of the dust transported to the Tacheng basin.

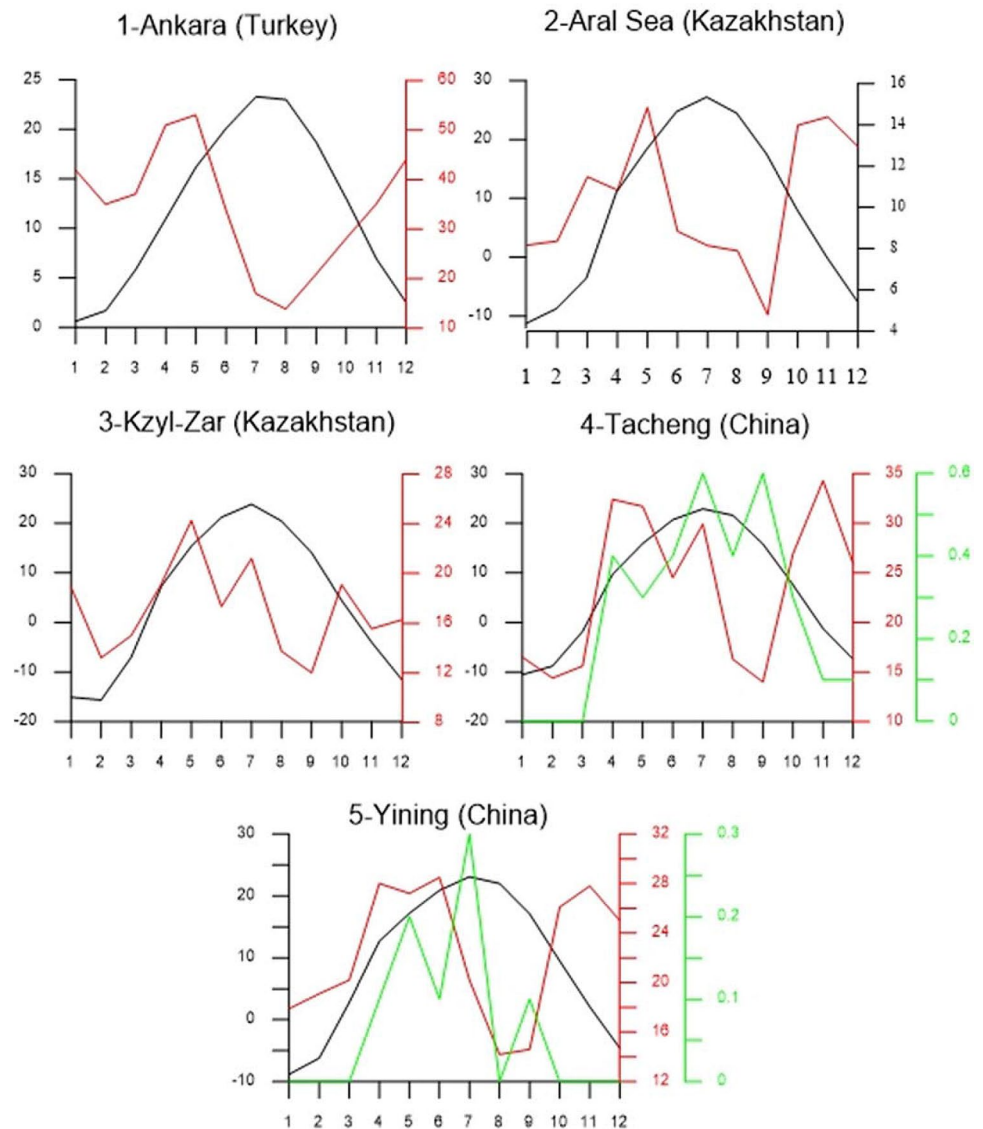
3 Methods

3.1 Sediment dating

All OSL samples were collected in light-tight steel tubes, sealed in black plastic bags to avoid light and water loss. Sample preparation and measurements were carried out under subdued red light in the Luminescence Dating Laboratory of the Qinghai Institute of Salt Lakes, Chinese Academy of Sciences. In laboratory, sediments at two ends of the tube, which may have been exposed to daylight during sampling, were scraped away and were used for radioisotope (U, Th and K) concentration measurement, and the remainder of the unexposed materials in the middle part of the tube were prepared for OSL equivalent dose (D_e) estimation.

Quartz fraction of 38–63 μm was extracted by wet sieving after a series of treatments using 10% HCl and 30%

Fig. 2 Monthly mean precipitation (red curve, unit in mm/month), air temperature (black curve, unit in °C), and dust storm days (green curve, unit in day) from five meteorological stations in the westerlies dominating regions (site numbers are shown in Fig. 1)



H₂O₂ to remove organic material and carbonates, and 40% fluorosilicic acid to remove feldspars and alpha-irradiated outer layer. We use heavy liquids with densities of 2.62, 2.75, and 2.58 g/cm³ to separate the quartz and K-feldspar fractions. The silica saturated fluorosilicic acid (H₂SiF₆) was then used to treat 38–63 μm quartz for about 2 weeks, while the 63–90 μm quartz was etched with 40% HF for 60 min, and then treated with 10% HCl to remove any fluoride. The purity of extracted quartz was detected by IR stimulation. When the IR signal is obvious, the quartz particles were retreated with H₂SiF₆ or HF. Repeat these processes until the IR signal is negligible in order to avoid age underestimation. Quartz grains were then mounted on the center of stainless-steel discs (5 mm in diameter) with silicone oil.

OSL measurements were carried out using an automated Risø TL/OSL DA-20 reader. The OSL signal was detected by a 9235QA photomultiplier tube through a 7.5 mm Hoya

U-340 filter. Laboratory irradiation used a ⁹⁰Sr/⁹⁰Y beta source. OSL stimulation was carried out for 40 s at 130 °C. The stimulation used blue LEDs (λ = 470 ± 20 nm) for quartz OSL. A *α* value of 0.035 ± 0.003 was used for 38–63 μm quartz (Lai et al. 2008). A combination of single aliquot regenerative-dose (SAR) protocol (Murray and Wintle 2000) and standardized growth curves (SGCs) (Lai 2006) was used for 20 samples De determination. For each sample, six aliquots were tested by SAR to establish an SGC, and then 12–16 additional aliquots were tested by SGC. The final De for each sample was derived from the mean of the SAR De and the SGC De. The net quartz OSL signals of the initial 0.64 s of stimulation were integrated for decay curve construction after subtraction of the last 8 s signals.

Typical OSL decay curves and growth curves of sample TC-10 and YM-6.5 are shown in Fig. 4. The blue-light stimulated OSL signals decrease rapidly during the first second

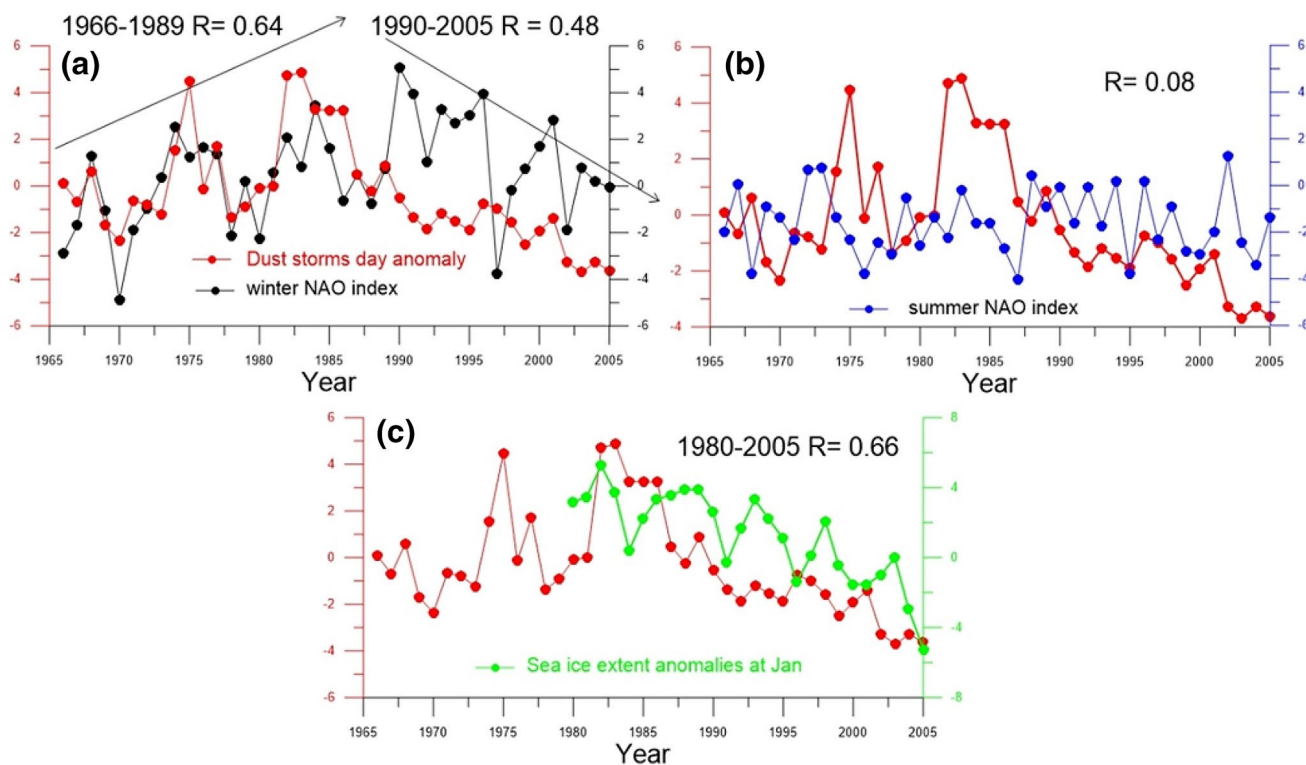


Fig. 3 Annual timescale comparison of the winter/summer NAO index, sea ice index at January, annual dust storm day anomalies in Tacheng region during 1966–2005. The winter and summer NAO index used here was acquired from [https://climatedataguide.ucar](https://climatedataguide.ucar.edu/climate-data/hurrell-north-atlantic-oscillation-nao-index-station-based)

[edu/climate-data/hurrell-north-atlantic-oscillation-nao-index-station-based](https://climatedataguide.ucar.edu/climate-data/hurrell-north-atlantic-oscillation-nao-index-station-based). Tacheng City dust storms data are provided by the China Meteorological Administration. The sea ice index was acquired from https://nsidc.org/data/seaice_index

of stimulation, indicating that the signal is dominated by the fast component. The D_e and calculated quartz OSL age for each sample are listed in Table 1. For all samples, the concentration of U, Th and K was measured using neutron activation analysis of dried samples at the Chinese Atomic Energy Institute for calculating the environmental dose rate. Calculation of the cosmic dose rate was based on Prescott and Hutton (1994). Considering data from previous Xinjiang loess studies (Lai et al. 2012; Li et al. 2016a, b), we used a water content of $10 \pm 5\%$ in all dose rate calculations.

3.2 Climatic proxy measurements and their implications

After removing organic matter and carbonate, grain size distribution of the samples at 2-cm intervals was measured using Malvern 2000 laser instrument. The grain-size variations in the worldwide loess-paleosol records have been widely used as paleoclimate indicators for atmospheric circulation (wind strength) (An et al. 1991; Ding et al. 2005). The grain size records from the Chashmanigar and Ili loess reflects, both located in Central Asia, have been used to reflect the intensity of the winds (Ding et al. 2002; Li et al. 2016b). Considering the large latitudinal shift in the

westerlies in various timescales, large change in wind intensity at Techeng section could be explained by the latitudinal change of the westerlies, which is similar to many papers for the interpretation of the westerlies' latitudinal position (e.g., Nagashima et al. 2011). Moreover, the positive correlation between the NAO and the dust storm in Tacheng region (Fig. 3) further indicates the increases of the grain size in the Tacheng section are attributed to a northward shift in the westerlies, accompany with a positive mode of the NAO.

3.3 Model and experimental setup

To investigate the response of westerlies to insolation, we first performed sensitivity experiments with LOVECLIM, a three-dimensional Earth system model of intermediate complexity. The detailed description of the model can be found in Goosse et al. (2010). It capably reproduces the major characteristics of the observed climate both for present-day conditions and for key periods of the past (Yin and Berger 2012). In our study, the atmosphere, ocean and vegetation components are interactively used (Goosse et al. 2010). The same version of LOVECLIM has already be used to investigate the response of the southern westerlies to insolation forcing (Yin 2013). Two sensitivity experiments have been

Fig. 4 OSL characteristics (decay curves and growth curves) for sample TC-10 and sample YM-6.5

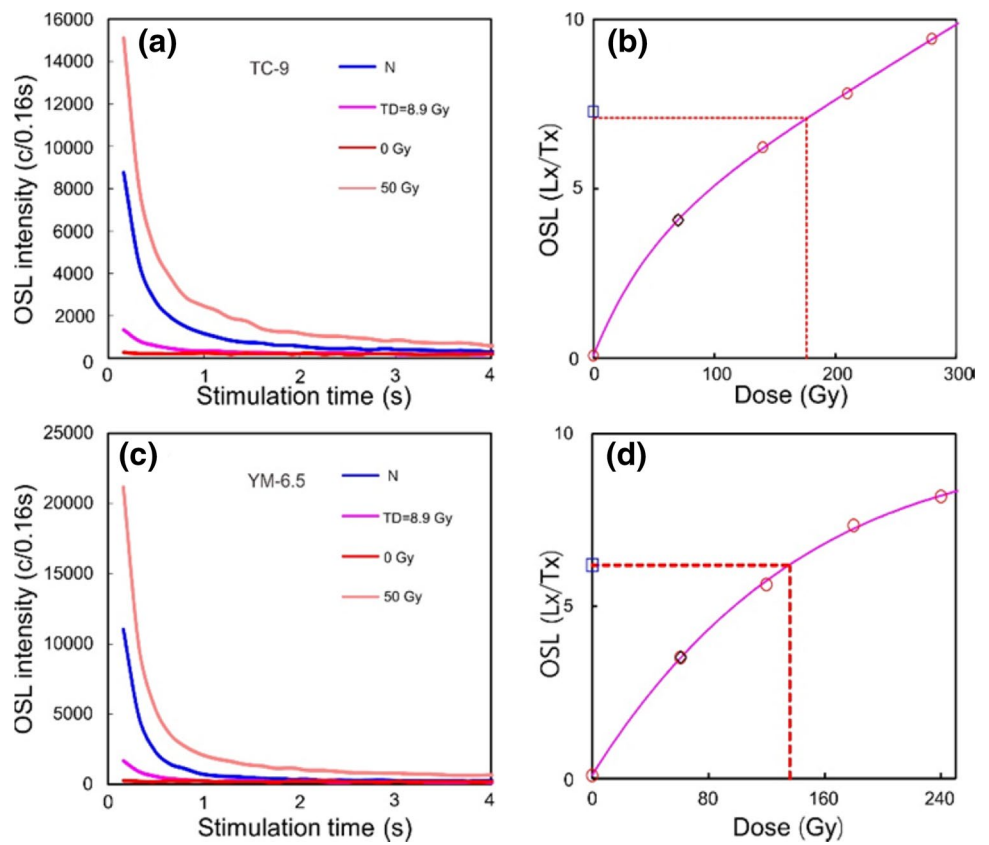


Table 1 Summary of dosimetry and OSL ages at Tacheng and Yumin section

Site	Sample no	U (ppm)	Th (ppm)	K (%)	Water content (%)	Dose rate (Gy/ka)	ED value (Gy)	OSL age (ka)
Tacheng	0.5	1.88	8.41	1.85	10±5	2.98±0.21	27.27±0.87	9.15±0.70
	1	2.17	8.23	1.83	10±5	3.01±0.21	50.02±2.70	16.63±1.69
	2	3.52	9.65	3.52	10±5	3.63±0.25	108.60±2.04	29.9±2.04 ^a
	3	3.12	9.22	2.03	10±5	3.45±0.24	83.95±2.22	24.33±1.96
	4	2.97	9.28	2	10±5	3.37±0.24	124.340±2.31	36.9±2.24 ^a
	5	2.69	10.2	2.02	10±5	3.36±0.24	119.55±2.51	35.50±2.71
	6	2.52	9.36	2.14	10±5	3.35±0.24	132.29±3.47	39.48±2.29
	7	2.41	9.36	1.99	10±5	3.18±0.23	142.17±3.06	44.75±2.61
	8	2.85	11.3	1.9	10±5	3.35±0.24	159.87±5.08	47.79±4.53
	9	2.63	11.3	2.14	10±5	3.49±0.25	176.23±6.59	51.01±3.24
	10	2.98	11.7	2.16	10±5	3.63±0.26	202.17±5.87	55.76±3.59
	11	3.16	13	2.34	10±5	3.93±0.28	236.82±6.12	60.32±4.43
	12	3.09	11.6	2.23	10±5	3.70±0.27	241.15±6.46	65.16±4.25
13	2.64	8.66	1.76	10±5	2.94±0.21	197.71±6.57	67.25±4.70	
13.4	2.55	8.21	1.96	10±5	3.06±0.22	204.36±6.35	68.39±4.16	
Yumin	0.5	2.08	8.81	1.95	10±5	3.14±0.22	40.92±0.87	13.03±0.94
	2.5	2.99	8.35	1.94	10±5	3.28±0.23	79.50±5.35	24.23±2.36
	4.5	2.53	8.39	1.90	10±5	3.04±0.22	91.01±4.21	29.91±2.55
	6.5	2.61	8.49	1.91	10±5	3.10±0.22	136.63±5.26	44.09±3.60
	8.5	2.66	10.70	1.90	10±5	3.25±0.23	162.95±5.85	50.18±4.04

^aTwo OSL dates are not used for chronology construction

performed. The first simulation (Exp. 1) is for the Pre-Industrial time when boreal summer is at aphelion (the longitude of perihelion = 102° , a precession maximum) (Berger 1978). The second one (Exp. 2) is the same as the first one except that boreal summer is at perihelion (the longitude of perihelion = 270° , a precession minimum).

In order to investigate the mid-latitude westerlies changes responding to a slowdown of the AMOC, we analyze the results of the TraCE-21 ka transient simulation driven by only freshwater forcing, which is a transient simulation of the global climate during the last 21,000 years (Liu et al. 2014). The TraCE-21 ka simulation was carried out using the Community Climate System Model version 3 (CCSM3), driven by realistic external climate forcing, including orbitally-induced insolation, greenhouse gas, meltwater fluxes and continental ice sheets. The full TraCE simulation has captured many key features of the reconstructed climate history since the last 21 ka, such as the North Atlantic climate (Liu et al. 2009, 2012), Southern Hemisphere climate (He 2010), El Niño variability (Liu et al. 2014) and East Asian monsoon (Wen et al. 2016).

4 Results and discussion

4.1 Loess chronology

The TC and YM OSL ages (Table 1) gradually increases with depth from ~ 10 to ~ 70 ka and from ~ 10 to ~ 60 ka, respectively. There is no obvious deposition discontinuity at the current OSL ages. Two OSL data at 2 and 4 m are

significantly reversed at the TC loess even when the dating errors are taken into account. We linearly fitted the ages of each sampling level between the independent OSL age controls after excluding two abnormal OSL age, and the $R^2 = 0.99$ and 0.98 at TC and YM section, respectively (Fig. 5); this is precise enough for our study. Based on the OSL chronology, the sedimentation rate varies from 22 cm/kyr at Tacheng and 20 cm/kyr at Yumin.

4.2 Paleoclimate index comparison

The grain size of the TC and YM loess show similar variability at both millennial and orbital time scales (Fig. 6). To investigate the factors that directly and indirectly control the mid-latitude westerlies during the last glacial age, we compare the Tacheng loess records with other climatic records including North Greenland ice core temperature (North Greenland Ice Core Project 2004), AMOC proxies (Henry et al. 2016) and sea ice (Hoff et al. 2016) in the North Atlantic, and the Mediterranean Sea speleothems $\delta^{13}\text{C}$ (Bar-Matthews et al. 2003; Fleitmann et al. 2009). The European stalagmite $\delta^{13}\text{C}$ values are controlled by the type and density of vegetation and are suggested to reflect local temperature/humidity variations (Fleitmann et al. 2009). The present-day and last glacial climates of Black Sea and east Mediterranean Sea are controlled by seasonal changes in the position and strength of the westerlies storm tracks (Kwiecien et al. 2009). Therefore, the Sofular/Soreq stalagmite $\delta^{13}\text{C}$ can indicate the latitudinal change the mid-latitude westerlies associated with the North Atlantic climatic changes, that is, high $\delta^{13}\text{C}$ values correspond to relatively dry conditions, a

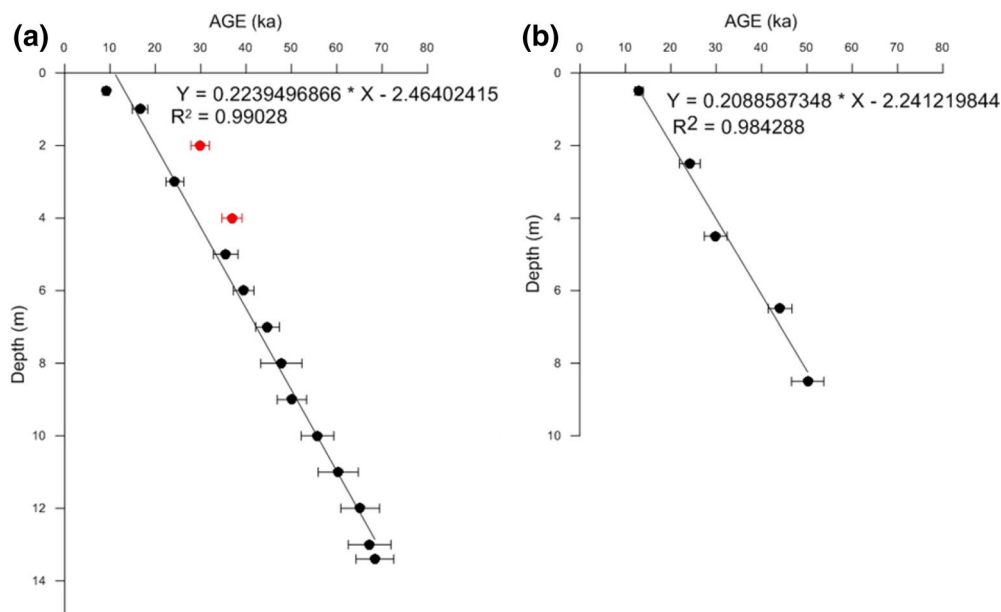
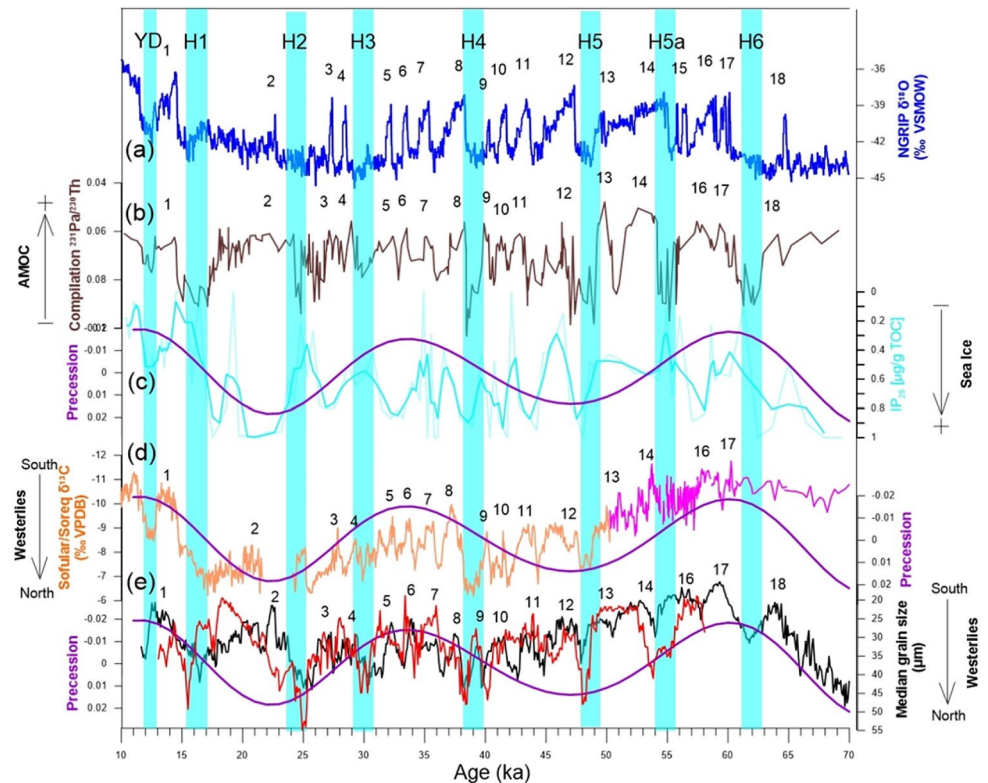


Fig. 5 Linearly fitted age-depth model for Tacheng (a) and Yumin (b) loess section

Fig. 6 a The last glacial data comparison. NGRIP $\delta^{18}\text{O}$ (blue) (North Greenland Ice Core Project 2004), b AMOC proxy (brown) (Henry et al. 2016), c Sea ice (cyan) (Hoff et al. 2016), d Sofular/Soreq $\delta^{13}\text{C}$ (orange/pink) (Bar-Matthews et al. 2003; Fleitmann et al. 2009), and e Median grain size of Tacheng and Yumin (black and red, this study), and the precession (purple) (Berger 1978). Sky-blue bars denote the Heinrich-like events identified in the six records. Black numbers (1–18, 10–70 kyr) denote well aligned DO events identified in the four records



NAO+ mode and a northward displacement of the westerlies (Voskresenskaya and Maslova 2011).

The increases of the grain size of the TC and YM section around 16, 24, 30, 39, 48, 55 and 62 kyr BP correspond well to the North Atlantic Heinrich events H_1 – H_6 , although the amplitude of coarsening grain size around 16, 25, 48 and 55 at the YM section is bigger than that of the TC section. Within the OSL ages error, they correspond to cooling over Greenland and weaker AMOC and a northward shift of the westerlies in the Mediterranean Sea and the Central Asia. Many of the millennial-scale events (DO 1–18) are well aligned in time between the loess, the speleothems and the AMOC records from the North Atlantic (Fig. 6), although the DO-2 and 15 events in the TC section, and DO-2, 10 and 13 events in the YM section are not well matched among them.

4.3 Forcing mechanism on millennial-orbital time scale

At the millennial time scale, to examine the mid-latitude westerlies in response to AMOC, we analyze the mid-latitude westerlies between the Heinrich 1 (H1) and the Bølling–Allerød (BA) event using only freshwater-forcing results from the TraCE-21 ka transient simulation (Fig. 7a). The slowdown of the AMOC weakens the global northward ocean heat transport, and induces the dipole SST anomaly in the Atlantic (Zhang and Delworth 2005). It also causes

the southward extension of sea ice during winter and spring, which leads to an intense cooling in the high-latitude North Atlantic (Wu et al. 2008). Consequently, temperatures in the high-latitude northern hemisphere decreased, leading to an increase in the meridional temperature gradient (Fig. 7c) and a high-pressure anomaly in the middle latitude and a low pressure one over the pole (Fig. 7b). These lead to a northward displacement of the westerlies in the mid-latitudes at 500 hPa (Fig. 7a), which is consistent with NAO+ mode from an AMOC shutdown experiment using FOAM model (Wu et al. 2008).

At the orbital time scale, the variation of the westerlies over Central Asia and the Mediterranean Sea follows well precession (Fig. 6), a northward shift of the westerlies corresponding to larger precession index (it means weaker summer insolation and stronger winter one in the NH), and vice versa. This indicates that precession and insolation control the variation of the westerlies at the orbital time scale. The difference in the latitudinal-seasonal insolation distribution between the two experiments due to the difference in precession is shown in Fig. 8. As compared to Exp. 2, there is less (more) insolation in Exp. 1 over the whole Earth during boreal summer (winter) especially in the mid and high latitudes of the northern (southern) hemisphere.

As the westerlies are the strongest and most zonal in winter which is a main factor for loess deposits in Tacheng, here we focus on the winter climate fields. Figure 9a shows that, in agreement with the Tacheng loess records and

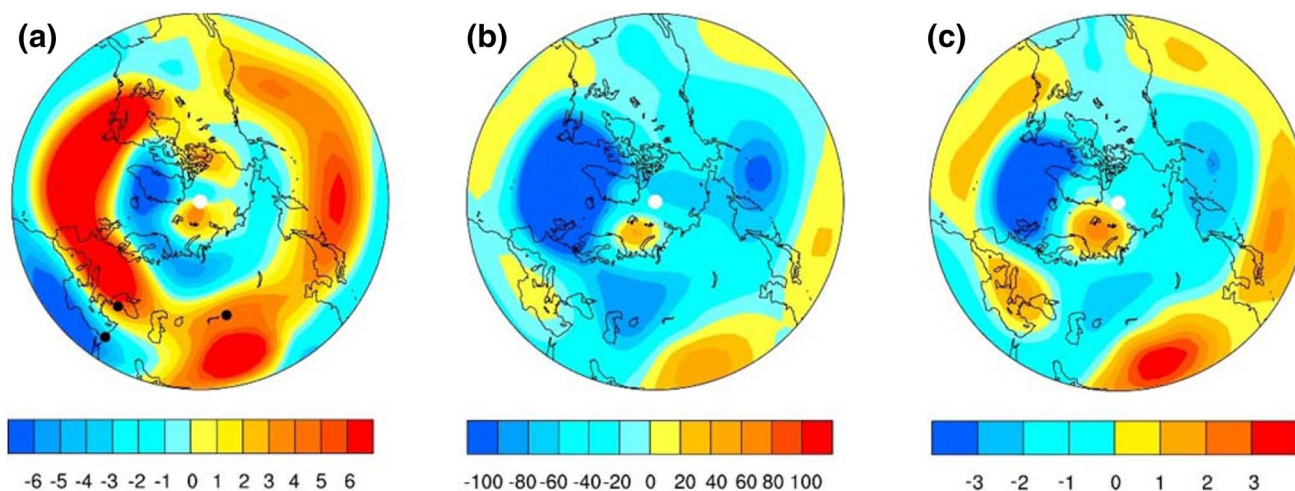


Fig. 7 The difference between H1 and BA in the zonal winds (m/s) (a), geopotential (m^2/s^2) (b) and air temperature ($^{\circ}\text{C}$) (c) at 500 hPa during winter (December–January–February), and the locations of

the Tacheng loess site, Sofular speleothem (Fleitmann et al. 2009), Soreq speleothem (Bar-Matthews et al. 2003)

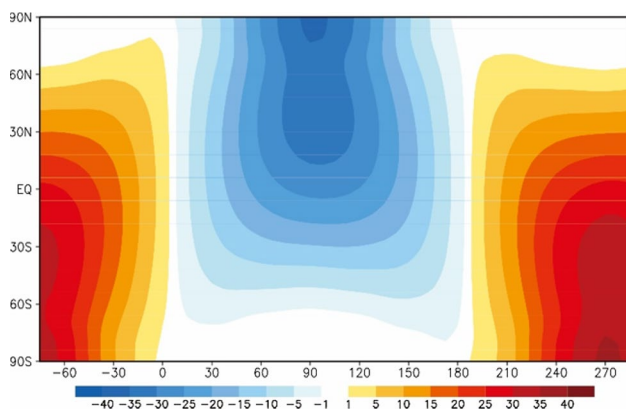


Fig. 8 Difference (Wm^{-2}) in the latitudinal–seasonal distribution of insolation between Exp. 1 and Exp. 2 (Exp. 1 minus Exp. 2). The x-axis gives the longitude ($^{\circ}$) of the Earth on its orbit (0° = spring equinox, 90° = summer solstice, 180° = fall equinox, 270° = winter solstice). The y-axis gives the latitude from the North Pole to the South Pole

other mid-latitudes ones, the model simulates a northward displacement of the westerlies in Exp. 1 when precession reaches a maximum, accompany with the NAO+ mode. These westerlies result from a larger latitudinal pressure gradient. Figure 9b shows that as compared to Exp. 2, the subtropical high gets intensified and the subpolar low gets much deepened in Exp. 1, leading to a larger latitudinal pressure gradient. The larger latitudinal pressure gradient is linked to a larger latitudinal temperature gradient. As compared to Exp. 2, the temperature in the mid latitudes increases in Exp. 1 but it decreases in the polar high latitudes (Fig. 9c), leading to a larger latitudinal temperature gradient (Fig. 9b). The temperature change can be explained by the difference in

insolation between the two experiments. During boreal winter, the mid-latitudes in Exp. 1 receive more insolation than in Exp. 2 (Fig. 8), making these latitudes warmer in winter. However, in the high latitudes, the energy is near zero in winter, therefore the winter temperature change in the polar region is attributed to the change in the local summer insolation, a phenomenon which has been called the summer remnant effect of insolation (Yin and Berger 2012). The polar region of Exp. 1 is much less insolated than Exp. 2 during boreal summer. This signal is transferred into local winter to reduce the air temperature through ocean-sea ice-atmosphere interactions (Yin and Berger 2012). Moreover, the sea ice during the last 70 ka is also controlled by the precession (Lo et al. 2018) (Fig. 6). When precession reaches a minimum, the sea ice loss will induce weaker poleward temperature/pressure gradient and weaker zonal winds aloft via thermal wind because of Arctic amplification (Overland et al. 2016). This similarity between the sea ice, the mid-latitude westerlies and precession also support that the precession drives the mid-latitude westerlies.

5 Conclusion

Both proxy records and model results show that, at the millennial and orbital time scale, the westerlies are controlled by AMOC and precession, respectively. A larger precession/smaller AMOC index leads to a northward displacement of westerlies through its influence on the latitudinal temperature and pressure gradients. Given the projected AMOC reduction over the next century, these gradients and consequently, the westerlies would move north in the future (Fischer et al. 2017).

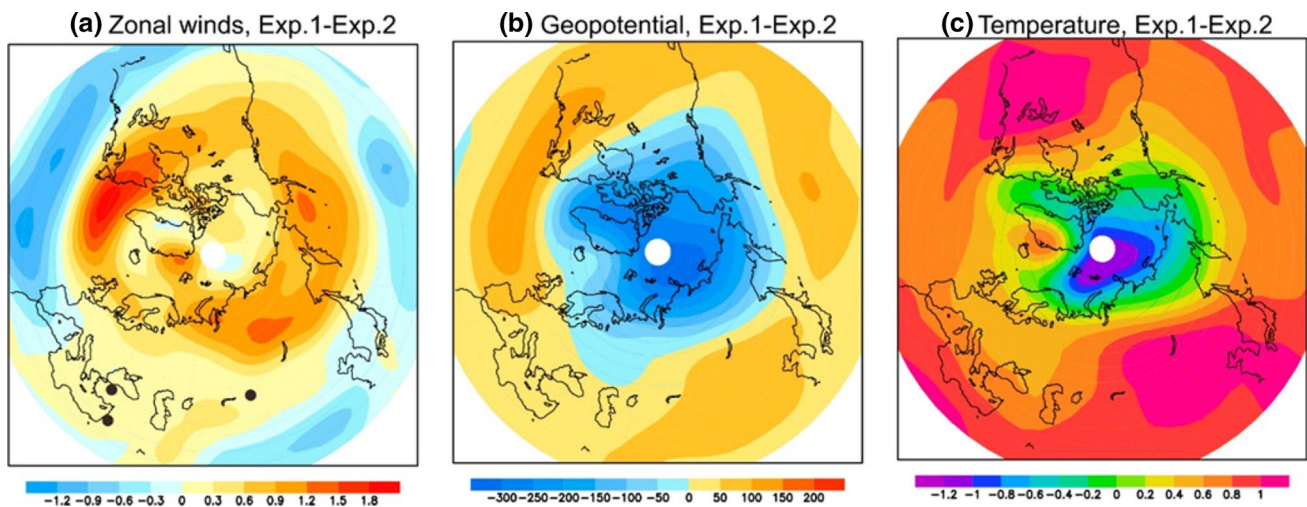


Fig. 9 The difference between Exp. 1 and Exp. 2 in the zonal winds (m/s), geopotential (m^2/s^2) and air temperature ($^{\circ}\text{C}$) at 500 hpa during winter (December–January–February)

Acknowledgements This work was supported by funds from the National Natural Science Foundation of China (NSFC Grant no. 41702189, 41572162), and the Fonds de la Recherche Scientifique-FNRS under Grant MIS F.4529.18. Q. Z. Yin is Research Associate of the Fonds de la Recherche Scientifique-FNRS.

References

- Aizen VB, Aizen EM, Melack JM (1996) Precipitation, melt and runoff in the northern Tien Shan. *J Hydrol* 186:229–251. [https://doi.org/10.1016/S0022-1694\(96\)03022-3](https://doi.org/10.1016/S0022-1694(96)03022-3)
- An Z, Kukla G, Porter SC, Xiao J (1991) Late quaternary dust flow on the Chinese loess plateau. *Catena* 18:125–132. [https://doi.org/10.1016/0341-8162\(91\)90012-M](https://doi.org/10.1016/0341-8162(91)90012-M)
- Bar-Matthews M, Ayalon A, Gilmour M, Matthews A, Hawkesworth CJ (2003) Sea–land oxygen isotopic relationships from planktonic foraminifera and speleothems in the Eastern Mediterranean region and their implication for paleorainfall during interglacial intervals. *Geochim Cosmochim Acta* 67:3181–3199. [https://doi.org/10.1016/S0016-7037\(02\)01031-1](https://doi.org/10.1016/S0016-7037(02)01031-1)
- Berger A (1978) Long-term variations of daily insolation and quaternary climatic changes. *J Atmos Sci* 35:2362–2367. [https://doi.org/10.1175/1520-0469\(1978\)035%3C2362:ltvodi%3E2.0.co;2](https://doi.org/10.1175/1520-0469(1978)035%3C2362:ltvodi%3E2.0.co;2)
- Brauer A, Haug GH, Dulski P, Sigman DM, Negandank JFW (2008) An abrupt wind shift in western Europe at the onset of the Younger Dryas cold period. *Nat Geosci* 1:520–523. <https://doi.org/10.1038/ngeo263>
- Clement AC, Peterson LC (2008) Mechanisms of abrupt climate change of the last glacial period. *Rev Geophys* 46:RG4002. <https://doi.org/10.1029/2006RG000204>
- Dansgaard W, Johnsen SJ, Clausen HB, Dahl-Jensen D, Gundestrup NS, Hammer CU, Hvidberg CS, Steffensen JP, Sveinbjornstottir AE, Jouzel J, Bond G (1993) Evidence for general instability of past climate from a 250-kyr ice-core record. *Nature* 364:218–220. <https://doi.org/10.1038/364218a0>
- Ding Z, Ranov V, Yang S, Finaev A, Han J, Wang G (2002) The loess record in southern Tajikistan and correlation with Chinese loess. *Earth Planet Sci Lett* 200:387–400. [https://doi.org/10.1016/S0012-821X\(02\)00637-4](https://doi.org/10.1016/S0012-821X(02)00637-4)
- Ding Z, Derbyshire E, Yang S, Sun J, Liu T (2005) Stepwise expansion of desert environment across northern China in the past 3.5 Ma and implications for monsoon evolution. *Earth Planet Sci Lett* 237:45–55. <https://doi.org/10.1016/j.epsl.2005.06.036>
- Fischer M, Domeisen DIV, Müller WA, Baehr J (2017) Changes in the seasonal cycle of the Atlantic meridional heat transport in a RCP 8.5 climate projection in MPI-ESM. *Earth Syst Dyn* 8:129–146. <https://www.earth-syst-dynam.net/8/129/2017/>
- Fleitmann D, Cheng H, Badertscher S, Edwards R, Mudelsee M, Gökürk O, Fankhauser A, Pickering R, Raible CC, Matter A, Kramers J, Tüysüz O (2009) Timing and climatic impact of greenland interstadials recorded in stalagmites from northern turkey. *Geophys Res Lett* 36:L19707. <https://doi.org/10.1029/2009GL040050>
- Goosse H, Brovkin V, Fichefet T, Haarsma R, Huybrechts P, Jongma J, Mochet A, Selten F, Barriat PY, Campin JM, Deleersnijder E, Driesschaert E, Goelzer H, Janssens I, Loutre MF, Morales Maqueda MA, Opsteegh T, Mathieu PP, Munhoven G, Pettersen EJ, Renssen H, Roche DM, Schaeffer M, Tartinville B, Timmerman A, Weber SL (2010) Description of the Earth system model of intermediate complexity LOVECLIM version 1.2. *Geosci Model Dev* 3:603–633. <https://doi.org/10.5194/gmd-3-603-2010>
- He F (2010) Simulating transient climate evolution of the last deglaciation with CCSM3. Ph. D thesis, Department of Atmospheric and Oceanic Sciences, University of Wisconsin-Madison, p 161
- Henry LG, McManus JF, Curry WB, Roberts NL, Piotrowski AM, Keigwin LD (2016) North Atlantic Ocean circulation and abrupt climate change during the last glaciation. *Science*. <https://doi.org/10.1126/science.aaf5529>
- Hoff U, Rasmussen TL, Stein R, Ezat MM, Fahl K (2016) Sea ice and millennial-scale climate variability in the Nordic seas 90 kyr ago to present. *Nat Commun* 7:12247. <https://doi.org/10.1038/ncomms12247>
- Hurrell JW, Van Loon H (1997) Decadal variations in climate associated with the north Atlantic oscillation. In: Diaz HF, Beniston M, Bradley RS (eds) *Climatic change at high elevation sites*. Springer, Dordrecht, pp 69–94. https://doi.org/10.1007/978-94-015-8905-5_4
- Kwiecien O, Arz HW, Lamy F, Plessen B, Bahr A, Haug GH (2009) North Atlantic control on precipitation pattern in the Eastern Mediterranean/Black Sea region during the last glacial. *Quat Res* 71:375–384. <https://doi.org/10.1016/j.yqres.2008.12.004>

- Lai Z (2006) Testing the use of an OSL standardised growth curve (SGC) for determination on quartz from the Chinese loess plateau. *Radiat Meas* 41:9–16. <https://doi.org/10.1016/j.radmeas.2005.06.031>
- Lai Z, Zöller L, Fuchs M, Brückner H (2008) Alpha efficiency determination for OSL of quartz extracted from Chinese loess. *Radiat Meas* 43:767–770. <https://doi.org/10.1016/j.radmeas.2008.01.022>
- Lai Z, Sun Y, Hou G, Yu L, Wu C (2012) A luminescence dating study of loess deposits from the Yili River basin in western China. *Quat Geochronol* 10:50–55. <https://doi.org/10.1016/j.quageo.2012.04.022>
- Li G, Rao Z, Duan Y, Xia D, Wang L, Madsen DB, Jia J, Wei H, Qiang M, Chen J, Chen F (2016a) Paleoenvironmental changes recorded in a luminescence dated loess/paleosol sequence from the Tianshan Mountains, arid Central Asia, since the penultimate glaciation. *Earth Planet Sci Lett* 448:1–12. <https://doi.org/10.1016/j.epsl.2016.05.008>
- Li Y, Song Y, Lai Z, Han L, An Z (2016b) Rapid and cyclic dust accumulation during MIS 2 in Central Asia inferred from loess OSL dating and grain-size analysis. *Sci Rep* 6:32365. <https://doi.org/10.1038/srep32365>
- Liu Z, Otto-Bliesner BL, He F, Brady EC, Tomas R, Clark PU, Carlson AE, Lynch-Stieglitz J, Curry W, Brook E, Erickson D, Jacob R, Kutzbach J, Cheng J (2009) Transient simulation of last deglaciation with a new mechanism for Bølling–Allerød warming. *Science* 325:310–314. <https://doi.org/10.1126/science.1171041>
- Liu Z, Carlson AE, He F, Brady EC, Otto-Bliesner BL, Briegleb BP, Wehrenberg M, Clark PU, Wu S, Cheng J, Zhang J, Noone D, Zhu J (2012) Younger Dryas cooling and the Greenland climate response to CO₂. *Proc Natl Acad Sci* 109:11101–11104. <https://doi.org/10.1073/pnas.1202183109>
- Liu Z, Lu Z, Wen X, Otto-Bliesner BL, Timmermann A, Cobb KM (2014) Evolution and forcing mechanisms of El Niño over the past 21,000 years. *Nature* 515:550. <https://doi.org/10.1038/nature13963>
- Lo L, Belt ST, Lattaud J, Friedrich T, Zeeden C, Schouten S, Smik L, Timmermann A, Cabedo-Sanz P, Huang J-J, Zhou L, Ou T-H, Chang Y-P, Wang L-C, Chou Y-M, Shen C-C, Chen M-T, Wei K-Y, Song S-R, Fang T-H, Gorbarenko SA, Wang W-L, Lee T-Q, Elderfield H, Hodell DA (2018) Precession and atmospheric CO₂ modulated variability of sea ice in the central Okhotsk Sea since 130,000 years ago. *Earth Planet Sci Lett* 488:36–45. <https://doi.org/10.1016/j.epsl.2018.02.005>
- Murray AS, Wintle AG (2000) Luminescence dating of quartz using an improved single-aliquot regenerative-dose protocol. *Radiat Meas* 32:57–73. [https://doi.org/10.1016/S1350-4487\(99\)00253-X](https://doi.org/10.1016/S1350-4487(99)00253-X)
- Nagashima K, Tada R, Tani A, Sun Y, Isozaki Y, Toyoda S, Hasegawa H (2011) Millennial-scale oscillations of the westerly jet path during the last glacial period. *J Asian Earth Sci* 40:1214–1220. <https://doi.org/10.1016/j.jseas.2010.08.010>
- North Greenland Ice Core Project Members (2004) High-resolution record of Northern Hemisphere climate extending into the last interglacial period. *Nature* 431:147. <https://doi.org/10.1038/nature02805>
- Overland JE, Dethloff K, Francis JA, Hall RJ, Hanna E, Kim S-J, Screen JA, Shepherd TG, Vihma T (2016) Nonlinear response of mid-latitude weather to the changing Arctic. *Nat Clim Change* 6:992. <https://doi.org/10.1038/nclimate3121>
- Prescott JR, Hutton JT (1994) Cosmic ray contributions to dose rates for luminescence and esr dating: Large depths and long-term time variations. *Radiat Meas* 23:497–500. [https://doi.org/10.1016/1350-4487\(94\)90086-8](https://doi.org/10.1016/1350-4487(94)90086-8)
- Son S-W, Lee S (2005) The response of westerly jets to thermal driving in a primitive equation model. *J Atmos Sci* 62:3741–3757. <https://doi.org/10.1175/jas3571.1>
- Sun Y, Clemens S, Morrill C, Lin X, Wang X, An Z (2012) Influence of Atlantic meridional overturning circulation on the East Asian winter monsoon. *Nat Geosci* 5:46–49. <https://doi.org/10.1038/ngeo1326>
- Voskresenskaya EN, Maslova VN (2011) Winter–spring cyclonic variability in the Mediterranean–Black Sea region associated with global processes in the ocean–atmosphere system. *Adv Sci Res* 6:237–243. <https://doi.org/10.5194/asr-6-237-2011>
- Wen X, Liu Z, Wang S, Cheng J, Zhu J (2016) Correlation and anticorrelation of the East Asian summer and winter monsoons during the last 21,000 years. *Nat Commun* 7:11999. <https://doi.org/10.1038/ncomms11999>
- Wu L, Li C, Yang C, Xie S-P (2008) Global teleconnections in response to a shutdown of the Atlantic meridional overturning circulation. *J Clim* 21:3002–3019. <https://doi.org/10.1175/2007JCLI1858.1>
- Yin J (2005) A consistent poleward shift of the storm tracks in simulations of 21st century climate. *Geophys Res Lett*. <https://doi.org/10.1029/2005GL023684>
- Yin Q (2013) Insolation-induced mid-Brunhes transition in Southern Ocean ventilation and deep-ocean temperature. *Nature* 494:222–225. <https://doi.org/10.1038/nature11790>
- Yin Q, Berger A (2012) Individual contribution of insolation and CO₂ to the interglacial climates of the past 800,000 years. *Clim Dyn* 38:709–724. <https://doi.org/10.1007/s00382-011-1013-5>
- Zhang R, Delworth TL (2005) Simulated tropical response to a substantial weakening of the Atlantic thermohaline circulation. *J Clim* 18:1853–1860. <https://doi.org/10.1175/JCLI3460.1>
- Zhang J, Peng G, Huang M, Zhang S (2006) Are dust storm activities in North China related to Arctic ice–snow cover? *Glob Planet Change* 52:225–230. <https://doi.org/10.1016/j.gloplacha.2006.02.007>

Publisher's Note Springer Nature remains neutral with regard to jurisdictional claims in published maps and institutional affiliations.